Journal of Applied Electrochemistry (2007) 37:275–282
DOI 10.1007/s10800-006-9254-4

Electrochemical removal of cadmium from dilute aqueous solutions using a rotating cylinder electrode of wedge wire screens

J.M. GRAU and J.M. BISANG*
Programa de Electroquímica Aplicada e Ingeniería Electroquímica (PRELINE), Facultad de Ingeniería Química (UNL), Santiago del Estero 2829, S3000AOM, Santa Fe, Argentina
*(*author for correspondence, e-mail: jbisang@fiqus.unl.edu.ar)*

Received 19 July 2006; accepted in revised form 2 October 2006

Key words: electrochemical reactor, mass transfer, rotating cylinder electrode, three-dimensional electrodes, wedge wire screens

Abstract

Rates of mass transfer at rotating cylinder electrodes of wedge wire screens were studied by measuring the limiting current for the cathodic reduction of ferricyanide as test reaction. The experimental data are well correlated by an empirical expression between the Sherwood number and the Reynolds number, both in terms of the internal slot opening as characteristic length, and including two additional dimensionless parameters in order to characterize the geometry of the screens. The performance of an undivided electrochemical batch reactor with a rotating cylinder cathode of wedge wire screens was tested analyzing the cadmium removal from dilute solutions. The effect of cathodic applied potential and size of the screen is studied. Taking into account the residual cadmium concentration the best results were obtained for a cathode potential of −1.1 V vs. SCE at 700 rpm, where the cadmium concentration decreased from 54 to 0.9 mg l^{-1} after 30 min of electrolysis with a specific energy consumption of 10.7 kWh kg^{-1} and a normalized space velocity of 3.54 h^{-1}.

List of symbols

a	constant in Equation 1
a_e	reactor specific surface area (m^{-1})
A	short mesh aperture in expanded metals (m)
A_s	electrode specific surface area (m^{-1})
C	concentration (mol m^{-3} or mg l^{-1})
d	external cylinder diameter (m)
d_h	hydraulic diameter $= 4\varepsilon/A_s$ (m)
D	diffusion coefficient (m^2 s^{-1})
E_s	specific energy consumption (W s mol^{-1} or kWh kg^{-1})
E_{SCE}	cathode potential referred to saturated calomel electrode (V)
F	Faraday constant (C mol^{-1})
H	distance between wires in woven-wire meshes (m)
I	current (A)
I_{lim}	limiting current (A)
k_m	mass-transfer coefficient (m s^{-1})
r_1	internal radius (m)
r_2	external radius (m)
$\bar{r}$	mean radius $= \sqrt{(r_1^2 + r_2^2)/2}$ (m)
R	external slot opening (m)
s_n	normalized space velocity (s^{-1} or h^{-1})
S	internal slot opening (m)
Re_d	Reynolds number in terms of d as characteristic length $= \omega\, r_2 d/\nu$
Re_S	Reynolds number in terms of S as characteristic length $= \omega\, r_2 S/\nu$
Sc	Schmidt number $= \nu/D$
Sh_d	Sherwood number in terms of d as characteristic length $= k_m d/D$
Sh_S	Sherwood number in terms of S as characteristic length $= k_m S/D$
t	time (min or s)
U	tangential velocity (m s^{-1})
U_c	cell voltage (V)
V	effective electrolyte volume within the reactor (m^3)
V_e	electrode volume (m^3)
WWS05	acronym of Wedge Wire Screen with a 0.5 mm internal slot opening
x	fractional conversion

Greek symbols

α	exponent of the Reynolds number in Equation 1
β	current efficiency (%)

γ	exponent of a dimensionless parameter in Equation 1
ε	porosity
κ	exponent of a dimensionless parameter in Equation 1
ν	kinematic viscosity ($m^2\ s^{-1}$)
ν_e	charge number of the electrode reaction
ρ_{mean}	space time yield ($kg\ m^{-3}\ s^{-1}$)
ω	rotation speed (rpm or s^{-1})

1. Introduction

Cadmium has a wide variety of applications such as rechargeable batteries, solar energy capture devices, coating of surfaces, alloys, pigments and stabilizers for plastics. However, these uses are affected by the toxicity of cadmium which produces environmental problems. The constant tightening of the standards for cadmium in waste water purification requires new measures to reduce the cadmium concentration. Recently, some authors have focused attention on the electrolytic treatment of cadmium. Dutra et al. [1] reported cadmium removal from acidic sulphate solutions by electrowinning in a divided flow-by cell with a reticulated vitreous carbon cathode. Efficient cadmium removal was only feasible in deaerated electrolyte. Thus, the cadmium concentration was decressed from 210 to 0.1 ppm in 85 min, with a current efficiency up to 40%, at a cathode potential of −0.89 V against the saturated calomel electrode. Tramontina et al. [2] demonstrated the feasibility of cadmium deposition at a reticulated vitreous carbon cathode from very dilute solutions with an initial cadmium concentration as low as 5 ppm. Elsherief [3] reported that, by using a flow-by cell with a spiral wound steel cathode, the cadmium concentration was decreased from 500 to 5 ppm in 90 min. Reade et al. [4] studied the removal of cadmium and copper with a reticulated vitreous carbon rotating cylinder electrode. A decrease in cadmium concentration from 56 ppm to less than 1 ppm was reported. Grau and Bisang [5, 6] studied cadmium removal with rotating cylinder electrodes. Using a continuous undivided electrochemical reactor with a rotating cylinder cathode of expanded metal a conversion per pass of 40% was achieved [7].

Wedge wire cylinders are produced by helically wrapping a triangular-shaped wire around parallel support rods to create a cylinder with continuous slot openings that widen inwardly so that particles tend to pass though the screen. The wires are automatically resistance welded to each support rod producing a very strong wedge wire cylinder with excellent beam, burst and collapse strength. The screens are non-plugging and self-cleaning. Likewise, the high open area contributes to low head losses through the screen surface. The screens are widely used in food and beverage processing, water intakes, fish diversion, architectural, and petrochemical applications as well as in many other applications involving liquid–solid and gas–solid separation [8].

Wedge wire cylinders present a higher specific surface area and their special structure promotes turbulence in the electrolyte flowing through them. However, the mass-transfer characteristics of the wedge wire screens have not been studied and the possibility to use these structures as three-dimensional electrodes has not been reported.

The aim of the present work is to analyse the behaviour of an undivided electrochemical reactor with a rotating wedge wire cylinder for the removal of cadmium and to perform a systematic study of the effect of the applied potential to the cathode. Special attention is paid to quantify the mass-transfer to the rotating cylinder electrode of wedge wire screens and to compare the mass-transfer characteristics with similar rotating structures.

2. Mass-transfer studies

2.1. *Theoretical aspects*

The mass-transfer at wedge wire cylinders can be studied taking into account the parameters k_m, U, ν, and D as single variables and introducing R, S, d_h, and d as geometric parameters in order to consider the characteristics of the structure. Performing a dimensional analysis results in the following dimensionless relationship

$$\frac{k_m S}{D} = a\left(\frac{US}{\nu}\right)^{\alpha} Sc^{1/3}\left(\frac{R+S}{S}\right)^{\gamma}\left(\frac{d_h}{d}\right)^{\kappa} \tag{1}$$

where the hydraulic diameter is given by

$$d_h = \frac{4\varepsilon}{A_s} \tag{2}$$

Considering that the tangential velocity is

$$U = \omega\frac{d}{2} \tag{3}$$

and defining a rotational Reynolds number as

$$Re_S = \frac{\omega d S}{2\nu} \tag{4}$$

gives

$$Sh_S = aRe_S^{\alpha}\ Sc^{1/3}\left(\frac{R+S}{S}\right)^{\gamma}\left(\frac{d_h}{d}\right)^{\kappa} \tag{5}$$

in which Sh_S and Re_S are the Sherwood and Reynolds numbers, respectively in terms of the internal slot opening as characteristic length.

2.2. *Experimental*

The experiments were performed in an undivided batch reactor (95 mm int. dia. and 140 mm high) maintained at a constant temperature by a heating jacket. Figure 1 shows the configuration of the electrochemical reactor used. The working electrode was a rotating cylinder made of wedge wire screens (WWS) of 304 stainless steel plated with nickel [9, 10]. The profile of the wires was flat top, 2 mm external width, 1 mm internal width and 3 mm wire height. The screen was supported by 14 rods of 3.25 mm diameter. Four types of screen were used; their geometrical characteristics, measured in the laboratory, are summarized in Table 1. The upper part of the electrode was joined to a Teflon sleeve in order to orientate the electrolyte flow through the screen. A perforated Teflon disc, positioned at the lower part of the electrode, was used as an additional support of the three-dimensional electrode. A nickel plated stainless steel bolt passed through the screen, pressing the electrode shaft and thus ensuring electric contact. A helical nickel wire (1.5 mm dia. $\times$ 190 cm long) with an interelectrode gap of 20 mm was used as counterelectrode. The working electrode and the counterelectrode were concentric, thereby ensuring a uniform primary current distribution. The reference electrode was a saturated calomel electrode and the potential was controlled against the reference electrode connected to a Luggin capillary positioned at the middle of the outer face of the three-dimensional cathode.

The test reaction was the electrochemical reduction of ferricyanide from solutions with $[K_3Fe(CN)_6] \cong 5 \times 10^{-4}$ M, $[K_4Fe(CN)_6] \cong 5 \times 10^{-2}$ M, in 1 M NaOH or 3 M NaOH as supporting electrolyte, while the reverse reaction occurs at the anode. Table 2 summarizes the composition and physicochemical properties of the solutions. The cathode potential was swept from the open circuit potential (typically 100 mV vs. SCE for 1 M NaOH and 125 mV for 3 M NaOH) to a value of -400 mV vs. SCE and the current against potential curve was then recorded at a sweep rate of 1 mV s^{-1}. In all cases a well defined limiting current was observed. Samples of the solution were taken from the reactor after each experiment and the ferricyanide concentration was spectrophotometrically determined using a Perkin–Elmer model Lambda 20 double-beam UV–Vis

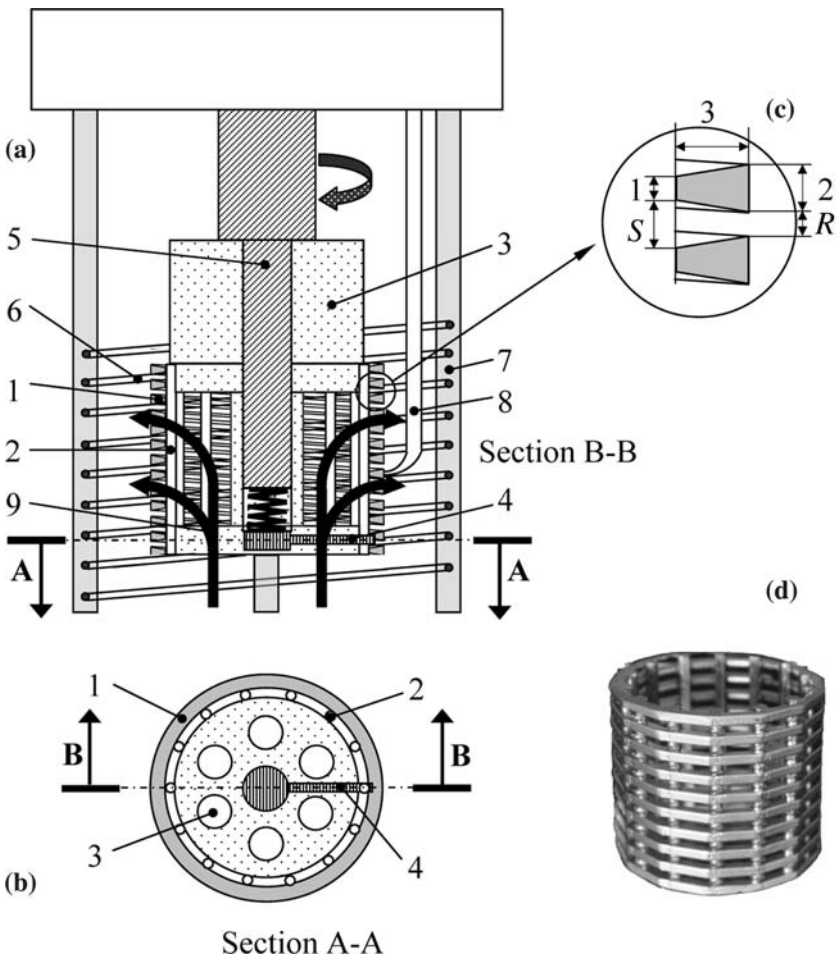

Fig. 1. (a) Cross-section of the electrochemical reactor. (1) working electrode, (2) support rods of the wedge wire screen, (3) Teflon sleeve, (4) electric contact, (5) electrode shaft, (6) anode, (7) anode support rods, (8) Luggin capillary and (9) electrolyte flow rate produced by the electrode rotation. (b) Plant view of the working electrode. (1) working electrode, (2) support rods of the wedge wire screen, (3) perforations in the Teflon disc to allow the electrolyte flow through the electrode, (4) electric contact. (c) Expanded view of wedge wire screen, characteristic parameters according to Table 1 and dimensions in mm. (d) Photograph of a wedge wire screen electrode.

Table 1. Geometrical parameters of the electrodes

Characteristic parameters of the wedge wire screens	WWS05	WWS10	WWS15	WWS20
External slot opening, R (mm)	0.5	1.0	1.5	2.0
Internal slot opening, S (mm)	1.5	2.0	2.5	3.0
External diameter, d (mm)	48.5	48.5	48	48.5
Thickness (mm)	3	3	3	3
Specific surface area, A_s (m^{-1})	885.56	772.55	737.87	631.37
Porosity, ε	0.476	0.537	0.551	0.612
Electrode length (mm)	39.80	40.70	40.45	41.40

Spectrophotometer with 10 mm glass absorption cells and as blank the supporting electrolyte was used. The measurements were performed at a wavelength of 430 nm, where it is possible to determine the ferricyanide concentration without interference of ferrocyanide. In a set of experiments the above procedure was repeated for five values of rotation speed in a given electrolyte. After two sets of experiments the nickel coating was stripped by acid immersion [11] and the electrode was plated with a fresh nickel surface. The experiments were performed at 30 °C and nitrogen was bubbled in the reactor for 1 h prior to the experiment in order to remove the dissolved oxygen.

In all the experiments the bed thickness of the three-dimensional electrode was 3 mm, which is lower than the value given by Kreysa [12]. Thus, the whole bed is working under limiting current conditions and the mass-transfer coefficient was calculated from the limiting current and reactant concentration using the following equation [13]

$$k_m = \frac{I_{lim}}{v_e F V_e A_s C}. \tag{6}$$

Further details of the electrode coating and electrolyte properties can be obtained from previous work [14].

2.3. *Mass-transfer results and comparisons*

The constant a and the exponents α, β, and κ in Equation 5 were determined using a linear multiparametric correlation adjusting the experimental points to the logarithmic form of Equation 5. Thus, the 40 experimental data of the present study fit the equation:

$$Sh_S = 0.0231 Re_S^{0.63} Sc^{1/3} \left(\frac{R+S}{S}\right)^{2.3} \left(\frac{d_h}{d}\right)^{-0.26} \tag{7}$$

with a correlation coefficient of 0.99 and 0.067 as standard deviation. Figure 2 compares the experimental results with the correlation values according to Equation 7. Attemps to obtain an empirical expression in terms of other relationships between the geometrical parameters did not produce a better correlation.

To provide comparison with existing mass-transfer data at rotating cylinder electrodes it is convenient to re-write Equation 7 with the Sherwood and Reynolds numbers in terms of the external cylinder diameter as characteristic length. Thus Equation 7 is transformed into

$$Sh_d = 0.0231 Re_d^{0.63} Sc^{1/3} \left(\frac{d}{S}\right)^{0.37} \left(\frac{R+S}{d}\right)^{2.3} \left(\frac{d_h}{d}\right)^{-0.26} \tag{8}$$

Equation 8 has the same form as the Eisenberg et al. [15] equation, valid for smooth rotating cylinder electrodes, multiplied by geometric parameters which take into account the characteristics of the wedge wire screen electrode.

In order to determine the efficiency of the wedge wire screens, a mass-transfer enhancement factor can be defined as the ratio between the mass-transfer coefficient for the three-dimensional electrode and the mass-transfer coefficient at a smooth rotating cylinder electrode [15]. The enhancement factor measures the improvement of the mass-transfer due to the turbulence promoting action of the three-dimensional structure. For the mass-transfer expressions proposed by Kreysa [16], Grau and Bisang [14, 17] and for Equation 8 in this study it is

Table 2. Properties of electrolytes

Composition	$[K_3Fe(CN)_6]$ $= 5 \times 10^{-4}$ M $[K_4Fe(CN)_6]$ $= 5 \times 10^{-2}$ M [NaOH] = 1 M	$[K_3Fe(CN)_6]$ $= 5 \times 10^{-4}$ M $[K_4Fe(CN)_6]$ $= 5 \times 10^{-2}$ M [NaOH] = 3 M	$[Cd^{+2}]$ = 50 mg l^{-1} $[Na_2SO_4]$ = 1 M pH≅7
Density (kg m^{-3})	1.05×10^3	1.12×10^3	1.11×10^3
Dynamic viscosity (kg m^{-1} s^{-1})	1.12×10^{-3}	1.55×10^{-3}	1.24×10^{-3}
Kinematic viscosity (m^2 s^{-1})	1.07×10^{-6}	1.38×10^{-6}	1.11×10^{-6}
Diffusion coefficient (m^2 s^{-1})	6.09×10^{-10}	4.40×10^{-10}	4.89×10^{-10}
Sc	1757	3136	2270

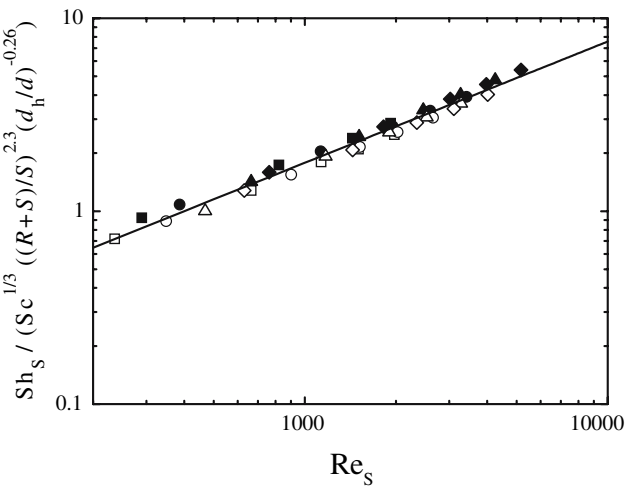

Fig. 2. Mass-transfer data against Reynolds number for the four types of electrodes. (■) WWS05, 1 M NaOH, (□) WWS05, 3 M NaOH, (●) WWS10, 1 M NaOH, (○) WWS10, 3 M NaOH, (▲) WWS15, 1 M NaOH, (△) WWS15, 3 M NaOH, (♦) WWS20, 1 M NaOH, (◇) WWS20, 3 M NaOH. Full line: Equation 7.

necessary to use a geometric factor which allows the correlations to be re-written in terms of the Sherwood and Reynolds numbers according to Eisenberg et al. [15]. Table 3 summarizes the mass-transfer correlations of three-dimensional rotating electrodes, which complements the information reported in previous works [14, 18]. A value of 1.05 was adopted for the geometric factor in the Kreysa equation, 0.42 for the relationship reported in Ref. [14], 1 for the correlation of the previous work [17] and 17.14 for the correlation of this study, which represent mean values for the geometrical arrays. Figure 3 shows the enhancement factor as a function of the Reynolds number, in terms of the cylinder diameter as characteristic length, at a Schmidt number of 2000 for different three-dimensional rotating structures. The enhancement factor for wedge wire screens ranges from 1.9 to 2.2, close to the values reported for reticulated vitreous carbon electrodes [19]. Likewise, the enhancement factor decreases when the Reynolds number increases, because the exponent of the Reynolds number for three-dimensional electrodes is lower than for smooth electrodes.

3. Removal of cadmium

3.1. *Experimental details*

The experiments were performed in the above reactor using as counterelectrode a concentric helical platinum wire (1 mm dia. × 50 cm long) with an interelectrode gap of 11 mm. The electrode reactions were oxygen evolution at the anode and cadmium deposition at the cathode. Likewise, hydrogen evolution and oxygen reduction occurred as cathodic side reactions. At high cadmium levels the oxygen reduction can be considered negligible due to the low value of the oxygen concentration, but it becomes more important at low metal concentration. The supporting electrolyte was 1 M Na_2SO_4, at pH ≅ 7, with an initial cadmium concentration of about 50 mg l^{-1}, the exact value was determined at each experiment. The solution volume in each experiment was 0.7 l. Samples of solution were taken from the reactor and the cadmium concentration was spectrophotometrically determined using the dithizone method [20]. From the temporal variation of concentration, current and cell voltage the current efficiency, the space time yield, the normalized space velocity and the specific energy consumption were calculated. All experiments were performed at 30 °C under potentiostatic control for 30 min at 700 rpm.

3.2. *Evaluation of the reactor performance*

For a rotating cylinder electrode the electrolyte is assumed to be well-mixed at all times. Thus, for a batch reactor in the potential range where the cadmium deposition is mass-transfer controlled, the change of concentration with time is given by:

Table 3. Summary of mass-transfer correlations for three-dimensional rotating electrodes under the following form: $Sh_d = a\ Re_d^{\alpha}\ Sc^{\varepsilon} \times$ geometric factor

Electrode type	Equation	Validity range
Smooth electrodes [15]	$Sh_d = 0.0791\ Re_d^{0.7}\ Sc^{0.356}$	$112 < Re_d < 1.62 \times 10^5$, $2230 < Sc < 3650$
Reticulated vitreous carbon [19]	$Sh_d = 0.44\ Re_d^{0.63}\ Sc^{1/3}$	$10^3 < Re_d < 10^4$, $Sc = 2388$
Packed bed[a] [16]	$Sh_d = 0.454 Re_d^{0.58} Sc^{1/3} \times \left(\frac{d_h}{2\pi}\right)^{0.58} \left(\frac{d_h}{r_2 - r_1}\right)^{1.116} \frac{d}{d_h}$	$Re_d < 5 \times 10^5$, $Sc = 1670$
Expanded metal [14]	$Sh_d = 1.356 Re_d^{0.63} Sc^{1/3} \times \left(\frac{d_h}{2\pi}\right)^{0.63} \left(\frac{d}{r}\right)^{0.94} \frac{d}{d_h}$	$4.8 \times 10^3 < Re_d < 9.2 \times 10^4$, $1757 < Sc < 3136$
Woven-wire meshes [17]	$Sh_d = 0.967 Re_d^{0.58} Sc^{1/3} \times \left(\frac{d_h}{2\pi}\right)^{0.58} \left(\frac{d}{r}\right)^{0.47} \frac{d}{d_h}$	$4.1 \times 10^3 < Re_d < 1.2 \times 10^5$, $1757 < Sc < 3136$
Wedge wire screens	$Sh_d = 0.0231 Re_d^{0.63} Sc^{1/3} \times \left(\frac{d}{s}\right)^{0.37} \left(\frac{d+s}{d}\right)^{2.3} \left(\frac{d_h}{d}\right)^{-0.26}$	$7.6 \times 10^3 < Re_d < 8.6 \times 10^4$, $1757 < Sc < 3136$

[a]For channel Reynolds number zero, with $d_h = \varepsilon\ d_p/(1-\varepsilon)$, being d_p particle diameter.

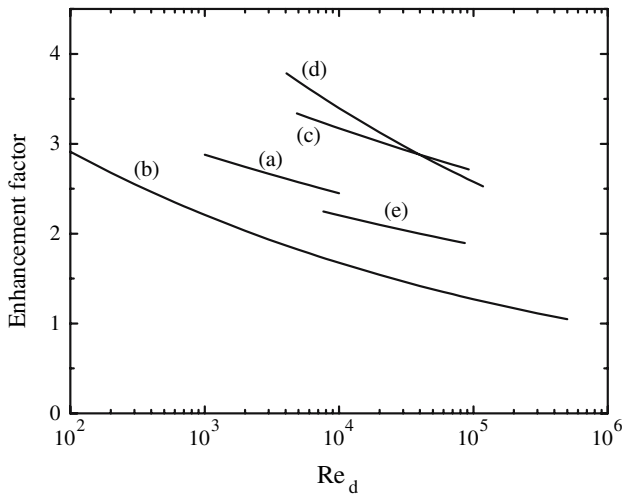

Fig. 3. Mass-transfer enhancement factor for three-dimensional rotating electrodes as a function of the Reynolds number in terms of the diameter of the electrode as characteristic length. Mass-transfer correlations according to Table 3. Sc = 2000. (a) Reticulated vitreous carbon [19]. (b) Packed bed [16]. (c) Expanded metal [14], (d) Woven-wire meshes [17] and (e) Wedge wire screens.

$$C(t) = C(0)\exp(-k_m a_e t). \tag{9}$$

The fractional conversion and the cumulative current efficiency as a function of time are given by:

$$x(t) = 1 - \exp(-k_m a_e t) \tag{10}$$

and

$$\beta(t) = \frac{v_e F V C(0) x(t)}{\int_0^t I(t)\mathrm{d}t} \tag{11}$$

Other "figures of merit" used to compare the performance of the electrochemical reactor are the mean value of the space time yield, the normalized space velocity and the specific energy consumption, which were calculated with the following equations:

$$\rho_{mean}(t) = \frac{C(0)x(t)}{t} \tag{12}$$

$$s_n(t) = -\frac{\ln[1 - x(t)]}{t \ln 10} \tag{13}$$

and

$$E_s(t) = \frac{\int_0^t U_c(t) I(t)\mathrm{d}t}{V C(0) x(t)}. \tag{14}$$

3.3. *Results and discussion*

Figure 4 shows the cadmium concentration as a function of time at different cathodic potentials. For a given potential, there is a pronounced decrease in concentration during the first stages of the experiments, but at high times the concentration approaches a constant value. The numbers at each experimental set are the final cadmium concentration. It can be observed that when the electrode potential decreases from −0.9 to −1.0 V the cadmium concentration also decreases. In the potential range from −1.0 to −1.2 V a small influence of the potential is observed. This behaviour can be explained by taking into account that for potentials more negative than −0.95 V the limiting current density is achieved [7]. At −1.3 V an increase in concentration is observed because at this potential hydrogen evolution is important and the deposited cadmium can be detached from the electrode and re-dissolved. Comparing Parts (a) and (b) of Figure 4 for a given potential it is observed that the decrease in concentration is higher for the WWS05 screen due to its higher specific surface area. The minimal residual cadmium concentration was lower than 1 mg l^{-1} obtained with the WWS05 screen for a cathode potential of −1.1 V after 30 min of electrolysis.

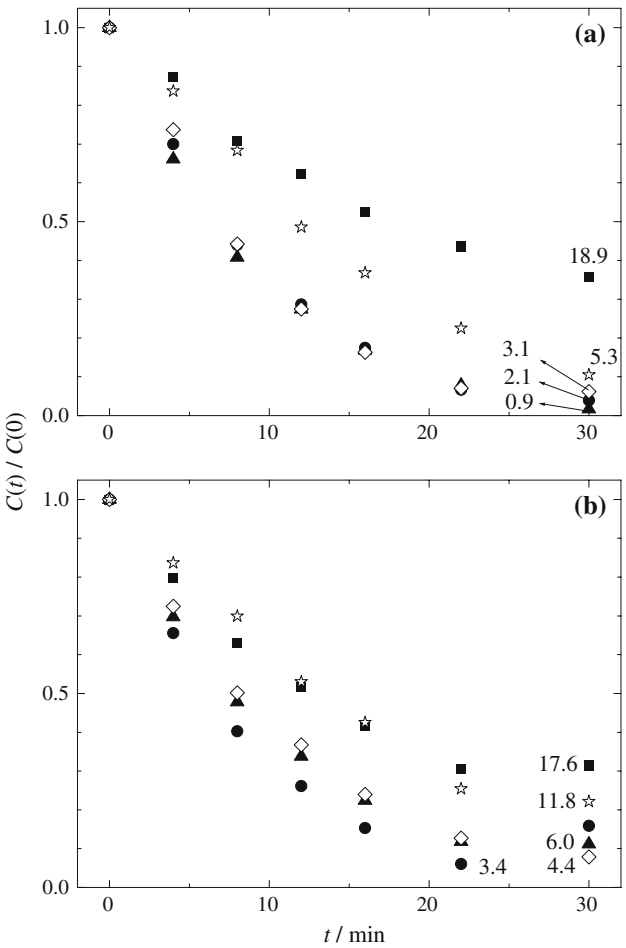

Fig. 4. Normalized cadmium concentration as a function of time. Part (a) WWS05. Part (b) WWS10. (■) E_{SCE} = −0.9 V, (●) E_{SCE} = −1.0 V, (▲) E_{SCE} = −1.1 V, (◇) E_{SCE} = −1.2 V, (☆) E_{SCE} = −1.3 V. ω = 700 rpm. T = 30 °C. Supporting electrolyte 1 M Na_2SO_4. $C(0) \cong 50$ mg l^{-1}. The number at each experimental set corresponds to the final cadmium concentration.

In Figure 5 the experimental results of Figure 4, obtained in the potential range of limiting current conditions for the WWS05 electrode, are re-plotted

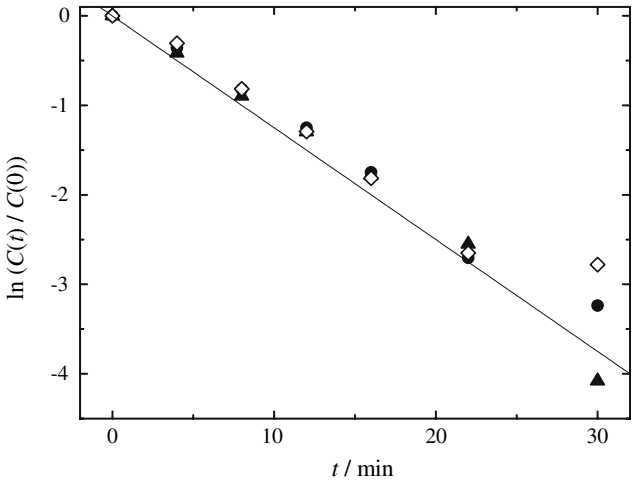

Fig. 5. Semi-logarithmic plot of normalized cadmium concentration as a function of time. WWS05 electrode. (●) $E_{SCE} = -1.0$ V, (▲) $E_{SCE} = -1.1$ V, (◇) $E_{SCE} = -1.2$ V. Full line: theoretical prediction according to Equations 7 and 9 in logarithmic form. $\omega = 700$ rpm. $T = 30$ °C. Supporting electrolyte 1 M Na_2SO_4. $C(0) \cong 50$ mg l^{-1}.

according to the dimensionless logarithmic form of Equation 9. The full line represents the theoretical behaviour with a mass-transfer coefficient calculated from Equation 7. Within the accuracy normally expected for this type of measurement the experimental results are in close agreement with the theoretical prediction mainly during the first stages of the experiments. For longer times, a higher discrepancy between experimental and predicted values is detected. This behaviour was also observed for copper [21] and tin [22] and can be attributed to the re-dissolution of the metal detached from the electrode.

Figure 6 shows typical curves of the cumulative current efficiency as a function of time for different cathode potentials for the WWS10 electrode. For a potential of −0.9 V the current efficiency is high at the beginning of the experiment and decreases with time because the cadmium concentration diminishes and oxygen reduction predominates as cathodic reaction. For more negative potentials the hydrogen evolution is more important as a cathodic side reaction and lower values of current efficiencies are measured.

Figure 7 shows the mean value of the space time yield and the normalized space velocity as a function of the applied potential when the charge passed in the reactor is about twice the stoichiometric value. A maximum in both figures of merit occurs when the cathodic potential is in the range −1.0 to −1.2 V. Therefore, this maximum may be a criterion for the choice of applied cathode potential.

Figure 8 shows the specific energy consumption as a function of time for different applied potentials. For a given potential, as the solution becomes more dilute the current efficiency decreases and the energy con-

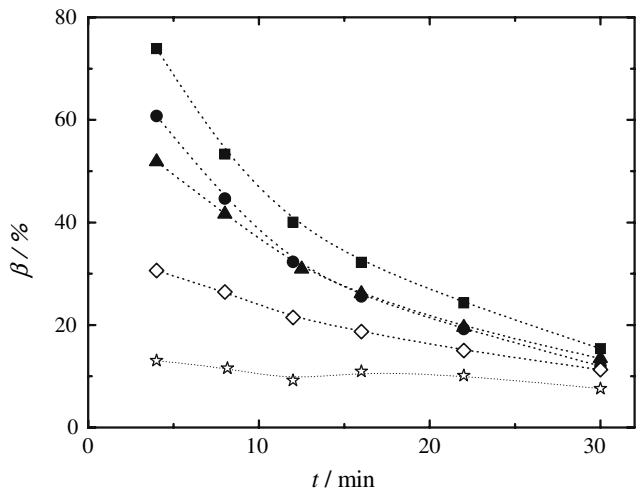

Fig. 6. Current efficiency as a function of time for different cathodic applied potentials. WWS10 electrode. (■) $E_{SCE} = -0.9$ V, (●) $E_{SCE} = -1.0$ V, (▲) $E_{SCE} = -1.1$ V, (◇) $E_{SCE} = -1.2$ V, (☆) $E_{SCE} = -1.3$ V. $\omega = 700$ rpm. $T = 30$ °C. Supporting electrolyte 1 M Na_2SO_4. $C(0) \cong 50$ mg l^{-1}.

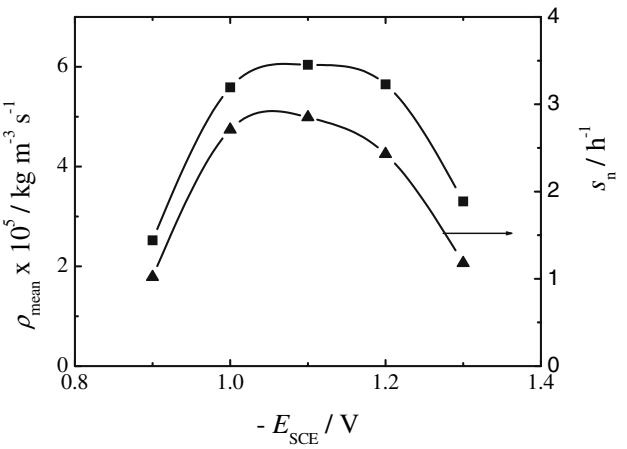

Fig. 7. Mean value of the space time yield and normalized space velocity as a function of the cathodic applied potential. WWS05 electrode. (■) ρ_{mean}, (▲) s_n. Ratio between the passed charge and the stoichiometric value ≅ 2. $\omega = 700$ rpm. $T = 30$ °C. Supporting electrolyte 1 M Na_2SO_4. $C(0) \cong 50$ mg l^{-1}.

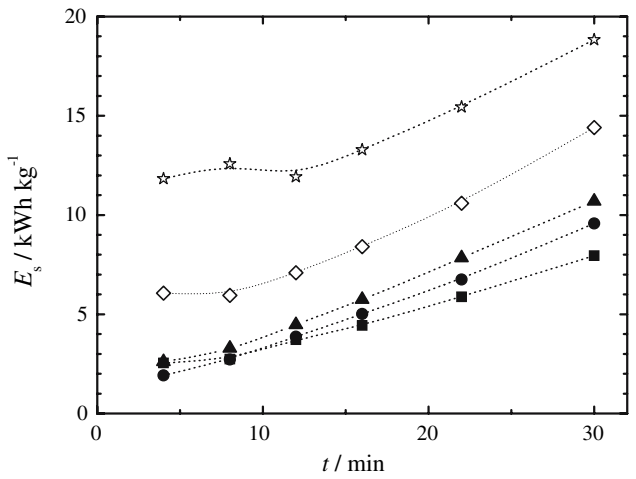

Fig. 8. Specific energy consumption as a function of time for different values of the cathodic applied potential. WWS05 electrode. (■) $E_{SCE} = -0.9$ V, (●) $E_{SCE} = -1.0$ V, (▲) $E_{SCE} = -1.1$ V, (◇) $E_{SCE} = -1.2$ V, (☆) $E_{SCE} = -1.3$ V. $\omega = 700$ rpm. $T = 30$ °C. Supporting electrolyte 1 M Na_2SO_4. $C(0) \cong 50$ mg l^{-1}.

sumption increases. The increase in E_s when the potential becomes more negative can be attributed to a decrease in current efficiency because of the onset of hydrogen evolution. The specific energy consumption is in accordance with values previously reported [3, 7, 23].

4. Conclusions

The following conclusions may be drawn:

(i) Mass-transfer at rotating cylinder electrodes of wedge wire screens is well correlated by a dimensionless equation involving the Sherwood and Reynolds numbers, in terms of the internal slot opening as characteristic length, the Schmidt number and two additional parameters characterizing the geometry of the three-dimensional structure.

(ii) The removal of cadmium from dilute aqueous solutions can be performed efficiently in an electrochemical reactor with a three-dimensional rotating cylinder electrode of wedge wire screens. Thus, the residual cadmium concentration was 0.9 mg l^{-1} for a cathode potential of −1.1 V against SCE, where the space time yield and the normalized space velocity achieve their maximum values.

(iii) The cadmium concentration follows the expected theoretical behaviour during the first stages of the experiment.

Acknowledgements

This work was supported by the Agencia Nacional de Promoción Científica y Tecnológica (ANPCyT), Consejo Nacional de Investigaciones Científicas y Técnicas (CONICET) and Universidad Nacional del Litoral (UNL) of Argentina. The authors are grateful to Model Chemical Laboratory (Facultad de Ingeniería Química-UNL) for the facilities to perform the spectrophotometric analysis and to INTECO S.R.L. for provision of the wedge wire screens.

References

1. A.J.B. Dutra, A. Espínola and P.P. Borges, *Minerals Eng.* **13** (2000) 1139.
2. J. Tramontina, D.S. Azambuja and C.M.S. Piatnicki, *J. Braz. Chem. Soc.* **13** (2002) 469.
3. E. Elsherief, *Electrochim. Acta* **48** (2003) 2667.
4. G.W. Reade, P. Bond, C. Ponce de Leon and F.C. Walsh, *J. Chem. Technol. Biotechnol.* **79** (2004) 946.
5. J.M. Grau and J.M. Bisang, *J. Chem. Technol. Biotechnol.* **76** (2001) 161.
6. J.M. Grau and J.M. Bisang, *J. Chem. Technol. Biotechnol.* **77** (2002) 465.
7. J.M. Grau and J.M. Bisang, *J. Chem. Technol. Biotechnol.* **78** (2003) 1032.
8. P.S. Ramachandran, *Chem. Eng. World* **38** (2003) 127.
9. L.J. Durney, *in* 'Ullmann's Encyclopedia of Industrial Chemistry', (VCH Verlagsgesellschaft, Weinheim, 1987), p. 142.
10. H. Brown and B.B. Knapp, *in* F.A. Lowenheim (ed.), 'Modern Electroplating', 3rd edn., Ch. 12, (John Wiley & Sons, New York, 1974), p. 292.
11. E.B. Saubestre, *in* F.A. Lowenheim (ed.), 'Modern Electroplating', 3rd edn., Ch. 32, (John Wiley & Sons, New York, 1974), p. 762.
12. G. Kreysa, *DECHEMA Monogr.* **94** (1983) 123 (in German).
13. F.C. Walsh, *A First Course in Electrochemical Engineering, Ch. 5* (Alresford Press, Alresford, 1993), pp. 149.
14. J.M. Grau and J.M. Bisang, *J. Appl. Electrochem.* **35** (2005) 285.
15. M. Eisenberg, C.W. Tobias and C.R. Wilke, *J. Electrochem. Soc.* **101** (1954) 306.
16. G. Kreysa, *Chem.-Ing.-Tech.* **55** (1983) 23 (In German).
17. J.M. Grau and J.M. Bisang, *J. Appl. Electrochem.* **36** (2006) 759.
18. C.T. John Low, C. Ponce de Leon and F.C. Walsh, *Aust. J. Chem.* **58** (2005) 246.
19. A.H. Nahlé, G.W. Reade and F.C. Walsh, *J. Appl. Electrochem.* **25** (1995) 450.
20. J. Fries and H. Getrost, *Organic Reagents for Trace Analysis* (E. Merck, Darmstadt, 1977), p. 78.
21. D. Robinson and F.C. Walsh, *Hydrometallurgy* **26** (1991) 115.
22. J.C. Bazan and J.M. Bisang, *J. Appl. Electrochem.* **34** (2004) 501.
23. D.R. Gabe and F.C. Walsh, *Proc. Reinhardt-Schuhmann, Symp. Ser. Met. Soc. (AIME)* (1987) 775.